

Regular Article

Improved Three-Component Decomposition Technique for Forest Parameters Estimation from PolInSAR Image

Nguyen Ngoc Tan, Pham Minh Nghia, Bui Ngoc Thuy

Faculty of Radio-Electronics, Le Qui Don Technical University, Ha Noi, Vietnam

Correspondence: Nguyen Ngoc Tan, ngoctanbk46@gmail.com

Communication: received 2 January 2018, revised 28 May 2018, accepted 13 July 2018

Online publication: 27 October 2018, Digital Object Identifier: 10.21553/rev-jec.192

The associate editor coordinating the review of this article and recommending it for publication was Dr. Ha Hoang Kha.

Abstract– Polarimetric SAR interferometry (PolInSAR) is an efficient remote sensing technique that allows to extract forest heights by means of model-based inversion. Recently, there have been plenty of researches on the retrieval of vegetation parameters by single frequency single baseline PolInSAR, such as the ESPRIT method and three-stage inversion method. However, these methods have several shortcomings which tend to underestimate the forest height due to attenuations of the electromagnetic waves in the ground medium. In order to overcome these shortcomings, an improved three-component decomposition technique using PolInSAR image is proposed in this paper. By means of coherence set and a Newton-Raphson method, the proposed method improves the accuracy of forest height estimation. The proposed algorithm performance is evaluated with simulated data from PolSARProSim software and L-band PolInSAR image pair of Tien-Shan test site which is acquired by the SIR-C/X-SAR system.

Keywords– PolInSAR, Target decomposition, Adaptive decomposition, forest height estimation, Newton-Raphson method, coherence set.

1 INTRODUCTION

Polarimetric SAR Interferometry (PolInSAR) was first developed in 1997 using SIR-C L-band data [1]. It provides a useful tool for forestry parameters retrieval as it bears capabilities of both interferometric SAR and polarimetric SAR [2]. The polarimetric information can reflect the geometric structure and the physical characteristic of a target. Especially, polarimetric and interferometric SAR data have been desired for forest biomass estimation. PolInSAR has been widely noticed for next generation of SAR remote sensing technology. Several techniques have been proposed for the forest height estimation using single baseline PolInSAR approach, such as ESPRIT (Estimation of Signal Parameters via Rotational Invariance Techniques) method [3, 4], three-stage inversion method [5]. The three-stage inversion process is one of the most successful processes for inversion of forestry parameters using PolInSAR image, in which ground topography can be retrieved by using line fit and vegetation bias removal in stage 1 and stage 2, respectively. The three-stage process is used as the basis of estimating two other parameters, height and extinction. However, in three-stage inversion method, the estimation of ground phase is time-consuming and not very accurate. In addition, the three-stage inversion method requires multiple parameter least-square estimation which is complex and often becomes ill-conditioned. The ESPRIT technique can detect local scattering centers corresponding to the canopy top and ground in the forest area but detection accuracy of the technique becomes worse for dense forest regions due to strong volume scattering component.

This paper presents an improved three-component decomposition approach. Firstly, the ground topographic phase is estimated by means of coherence set [6]. Second, the parameters of the volume scattering component are determined by solving the cubic equation and the parameters of the dihedral scattering and surface scattering components are determined by the Newton-Raphson algorithm after the volume scattering component is removed. Finally, the forest height is estimated by phase differencing.

The organization of this paper is as following. In Section 2, we present the elementary scattering mechanisms for polarimetric interferometric observations and general volume scattering model. The improved three-component decomposition technique and estimation of forest parameters are proposed in Section 3. The experimental results of the proposed method with simulated data and space-borne data are presented and discussed in Section 4. Finally, the conclusion and future work are drawn in Section 5.

2 ELEMENTARY SCATTERING MECHANISMS AND GENERAL VOLUME SCATTERING MODEL

A full polarimetric interferometry system measures for each resolution element in the scene from two slightly different look angles, two scattering matrices $[S_1]$ and $[S_2]$. In the case of backscattering in a reciprocal medium, the 3-D lexicographic scattering vectors \vec{k}_{L_1} and \vec{k}_{L_2} are given by

$$\vec{k}_{L_1} = [S_{1HH}, S_{1HV}, S_{1VV}]^T; \vec{k}_{L_2} = [S_{2HH}, S_{2HV}, S_{2VV}]^T \quad (1)$$

The complex information measured by the SAR system can be presented in form of three 3×3 complex matrices $[C_{11}]$, $[C_{12}]$ and $[C_{22}]$ formed by using outer products of \vec{k}_{L_1} and \vec{k}_{L_2} as

$$\begin{aligned} [C_{11}] &= \langle \vec{k}_{L_1} \vec{k}_{L_1}^{*T} \rangle, \\ [C_{22}] &= \langle \vec{k}_{L_2} \vec{k}_{L_2}^{*T} \rangle, \\ [C_{12}] &= \langle \vec{k}_{L_1} \vec{k}_{L_2}^{*T} \rangle, \end{aligned} \quad (2)$$

where $\langle \cdot \rangle$ denotes the ensemble average in the data processing, and $*$ denotes the complex conjugation. $[C_{ii}]$ ($i = 1, 2$) are the conventional Hermitian covariance matrices that describe the polarimetric properties for each image separately, while $[C_{12}]$ is a non-Hermitian complex matrix that contains polarimetric and interferometric information.

In this paper, the cross correlation matrix $[C_{12}]$ will be expressed as the sum of three matrices accounting for the contributions of surface $[C_S]$, double bounce $[C_D]$ and volume $[C_V]$ as follows:

$$[C_{12}] = [C_S] + [C_D] + [C_V] \quad (3)$$

In which the component matrices are represented as follows:

a. Surface scattering model

The scattering matrix of Bragg surface for master and slave images can be expressed in simplified form as in [7, 8]

$$[S_S^1] = \begin{bmatrix} S_{HH}^1 & 0 \\ 0 & S_{VV}^1 \end{bmatrix} \quad (4)$$

and

$$[S_S^2] = \begin{bmatrix} S_{HH}^2 e^{-j\phi_S} & 0 \\ 0 & S_{VV}^2 e^{-j\phi_S} \end{bmatrix} \quad (5)$$

where ϕ_S denotes the interferometric phase for the surface scattering. We assume that the phase of the co-polarized components are the same for both images. In case of the C_{13} entry of the surface scattering matrix, (6) is obtained in [7, 8]

$$\begin{aligned} C_{13} &= \langle S_{HH}^1 (S_{VV}^2 e^{-j\phi_S})^* \rangle \\ &= \langle |S_{HH}^1| e^{j\phi_{1H}} |S_{VV}^2| e^{-j\phi_{2V}} e^{j\phi_S} \rangle \\ &= \langle |S_{HH}^1| |S_{VV}^2| e^{-j\phi_{HV}} e^{j\phi_S} \rangle, \end{aligned} \quad (6)$$

where the equivalence $|S_{HH}^1| = |S_{HH}^2| = |S_{HH}|$ and $|S_{VV}^1| = |S_{VV}^2| = |S_{VV}|$ are assumed and $\phi_{HV} = \phi_H - \phi_V$ is the phase difference between the different polarization channels. Therefore, the covariance matrix for the surface scattering contribution is expressed as in [7, 8]

$$\begin{aligned} C_S &= \begin{bmatrix} |S_{HH}|^2 e^{j\phi_S} & 0 & |S_{HH}| |S_{VV}| e^{j(\phi_{HV} + \phi_S)} \\ 0 & 0 & 0 \\ |S_{HH}| |S_{VV}| e^{j(-\phi_{HV} + \phi_S)} & 0 & |S_{VV}|^2 e^{j\phi_S} \end{bmatrix} \\ &= F_S \begin{bmatrix} |\beta|^2 & 0 & \beta^* \\ 0 & 0 & 0 \\ \beta & 0 & 1 \end{bmatrix}, \end{aligned} \quad (7)$$

where F_S and β are defined as: $F_S = |S_{VV}|^2 e^{j\phi_S}$ and $\beta = \frac{|S_{HH}|}{|S_{VV}|} e^{j(\phi_H - \phi_V)}$.

b. Double bounce scattering model

The double bounce scattering component is modeled by scattering from a dihedral corner reflector, including a double scattering interaction between the ground and tree-trunk or stem, where the reflector surface can be made of different dielectric materials.

The double-bounce scattering matrix $[C_D]$ is given as in [7, 8]

$$C_D = F_D \begin{pmatrix} |\alpha|^2 & 0 & \alpha \\ 0 & 0 & 0 \\ \alpha^* & 0 & 1 \end{pmatrix}, \quad (8)$$

where

$$F_D = |R_{GV} R_{TV}|^2 e^{j\phi_D}$$

and

$$\alpha = \frac{R_{GH} R_{TH}}{R_{GV} R_{TV}} e^{j(\phi_V - \phi_H)},$$

in which ϕ_D denotes the interferometric phase, and $\phi_V - \phi_H$ is the phase difference between the different polarization channels. R_{GH} and R_{GV} are the horizontal and vertical Fresnel reflection coefficients of the ground surface. Similarly, the vertical trunk surface has reflection coefficients R_{TH} and R_{TV} for horizontal and vertical polarizations, respectively. These coefficients are assumed to be equal for master and slave images.

c. General volume scattering model

In the case of vegetation model, the co-polar and cross-polar responses are uncorrelated and cross-polar response is generated by volume scatters [9, 10]. Under the reflection symmetry assumption for reciprocal media, general volume scattering model obeys the following expression [11].

$$[C_V(\delta)] = \frac{1}{\frac{3}{2}(1+\delta) - \frac{\sqrt{\delta}}{3}} \begin{bmatrix} \delta & 0 & \sqrt{\delta}/3 \\ 0 & \frac{1+\delta}{2} - \frac{\sqrt{\delta}}{3} & 0 \\ \sqrt{\delta}/3 & 0 & 1 \end{bmatrix} \quad (9)$$

with $\delta = \langle |S_{HH}|^2 \rangle / \langle |S_{VV}|^2 \rangle$.

The Equation (9) is applied to the PolSAR data. However, PolInSAR image is a coherent combination of two polarimetric SAR images by means of interferometry. PolInSAR combines the advantage of polarimetric SAR (PolSAR) and interferometric SAR (InSAR). So the scattering process from a random volume for PolSAR and PolInSAR is similar. With PolInSAR data, the amplitude of the scattering coefficients does not change for both images, being the difference just in the phase term. This phase term will have two contributions: the difference due to the complex scattering coefficient in case of using different polarizations $\phi_H - \phi_V$ and the interferometric phase related with the position in the vertical coordinate ϕ_V . Note that the phase center of the volume scattering will be assumed the same for all polarizations [7, 8]. So, the volume scattering matrix is described as

$$C_V = F_V [C_V(\delta)], \quad (10)$$

where $F_V = |f_v| e^{j\phi_v}$ with $f_v e^{j\phi_v}$ corresponds to contribution of the volume scattering component.

Under the reflection symmetry assumption for recip-

rocal medial, it is assumed that $|S_{1HH}| = |S_{2HH}| = |S_{HH}|$ and $|S_{1VV}| = |S_{2VV}| = |S_{VV}|$. Thus, with PolInSAR data, coefficient δ is expressed as

$$\begin{aligned} \delta &= \langle |S_{1HH}|^2 \rangle / \langle |S_{1VV}|^2 \rangle \\ &= \langle |S_{2HH}|^2 \rangle / \langle |S_{2VV}|^2 \rangle. \end{aligned} \quad (11)$$

3 IMPROVED THREE COMPONENT DECOMPOSITION TECHNIQUE FOR ESTIMATING VEGETATION HEIGHT

3.1 Ground Topography Estimation by Means of Coherence Set

Three-stage inversion process is a traditional way to retrieve forestry parameters by using PolInSAR image. However, it has some disadvantages, in which the estimation of ground phase is time-consuming and not very accurate. The inversion process employs several typical polarizations, such as HH , VV , HV , $HH + VV$, $HH - VV \dots$ to do the least square line fit for the extraction of the line segment. Then one of the pair phases is selected as the underlying ground topographic phase by vegetation bias removal. However, errors could be introduced in this ground topography estimation method since limited number of coherences is usually applied in line fit, while a large number of coherences will increase computational cost. The coherence set method is proposed to overcome shortcomings which occur in three-stage inversion process. The topography will be estimated directly from the data itself and unambiguous values will be obtained by using all the polarimetric variations of interferometric coherence without increasing computational cost. Thus, the coherence set method yields more accurate results than the three-state inversion process when estimating the ground phase.

For fully polarimetric SAR systems, the generalized vector expression for the coherence $\tilde{\gamma}$ is given by [1, 2]

$$\tilde{\gamma}(\omega_1, \omega_2) = \frac{\omega_1^H \Omega_{12} \omega_2}{\sqrt{\omega_1^H T_{11} \omega_1 \omega_2^H T_{22} \omega_2}} \quad (12)$$

Another representation of PolInSAR data, called coherence set, was presented in [12], in which a set whose members are the coherences for all the possible polarizations is used. With the assumption that projection vectors are equal ($\omega_1 = \omega_2 = \omega$), coupled with approximation that T_{11} and T_{12} are similar ($T_{11} = T_{12} = T$), the approximate coherence set is given:

$$\Gamma_{\text{app}} = \left\{ w^H \bar{\Pi} w : w^H w = 1, w \in \mathbb{C}^3 \right\} \quad (13)$$

with $\bar{\Pi} = T^{-1/2} \Omega_{12} T^{-1/2}$ and $w = \frac{\sqrt{T} \omega}{\omega^H \sqrt{T} \omega}$.

Equation (9) is closely related to the numerical range (NR) of a square matrix $A \in \mathbb{C}^{3 \times 3}$

$$F(A) = \left\{ x^H A x : x^H x = 1, x \in \mathbb{C}^3 \right\} \quad (14)$$

Hence, NR of Matrix $\bar{\Pi}$ can be considered as the coherence set region.

According to azimuth symmetry in natural distributed area ($\langle S_{hh} S_{hv}^* \rangle = \langle S_{hv} S_{vv}^* \rangle = 0$), $\bar{\Pi}$ can be rewritten as [12]:

$$\bar{\Pi} = \begin{bmatrix} a & b & 0 \\ c & d & 0 \\ 0 & 0 & e \end{bmatrix} = \begin{bmatrix} B \\ e \end{bmatrix}, \quad a, b, c, d \in \mathbb{C}, B \in \mathbb{C}^{2 \times 2} \quad (15)$$

NR hull of the complex 2×2 matrix B in Equation (11) is an ellipse with foci at the eigenvalues λ_1 and λ_2 of B ($\arg(\lambda_1) > \arg(\lambda_2)$). $\bar{\Pi}$ has three eigenvalues λ_1 , λ_2 and e . In fact, point e is an approximation of $\tilde{\gamma}_{hv}$, while λ_1 and λ_2 are related to $\tilde{\gamma}_{hh}$ and $\tilde{\gamma}_{vv}$. As we can see, λ_2 is always near the topography $e^{i\phi_0}$, hence there are two line structures ($\lambda_1 \lambda_2$ and $e \lambda_2$) in the coherence shape. Usually it is assumed that HV is taken to be complex volume coherence, as this channel is dominated by volume scattering. Using these properties, linear structure of the polarimetric variation of interferometric coherence can be estimated by simply linking point e and eigenvalue λ_2 , and then the ground topography can be retrieved using one of the intersections of the line and the unit circle.

3.2 An Improved Three Component Decomposition Method Extracting the Parameters of Three Scattering Components

Simple replacement of three scattering terms in Equation (3) by Equations (7), (8) and (10) provides the new formula as

$$[C_{12}] - F_v [C_V(\delta)] = \begin{bmatrix} |\alpha|^2 F_D + |\beta|^2 F_S & 0 & \alpha F_D + \beta^* F_S \\ 0 & 0 & 0 \\ \alpha^* F_D + \beta F_S & 0 & F_D + F_S \end{bmatrix} \quad (16)$$

We see that the determinant of the matrix on the right is zero. Hence, the above formula can be rewritten as follows:

$$|[C_{12}] - F_v [C_V(\delta)]| = 0 \quad (17)$$

Based upon the generalized model for volume scattering in (9), we develop (17) into a cubic equation. This equation is formed to find the parameters of the volume scattering component.

At first we analytically derived the solutions of this equation and f_v will correspond to the solution which has the greatest value. Power of volume scattering component can be derived by the coefficient f_v and the canopy phase ϕ_v can be defined as

$$\phi_v = \max \{ \arg(F_{v1}, F_{v2}, F_{v3}) \}, \quad (18)$$

where F_{vi} , ($i = 1, 2, 3$) are the solutions of the cubic equation.

Secondly, when the proper f_v and ϕ_v are selected, we can remove the volume scattering component from the original cross correlation matrix. The remainder matrix is presented as

$$\begin{aligned} [C_{\text{remainder}}] &= [C_S] + [C_D] \\ &= \begin{bmatrix} |\alpha|^2 F_D + |\beta|^2 F_S & 0 & \alpha F_D + \beta^* F_S \\ 0 & 0 & 0 \\ \alpha^* F_D + \beta F_S & 0 & F_D + F_S \end{bmatrix}. \end{aligned} \quad (19)$$

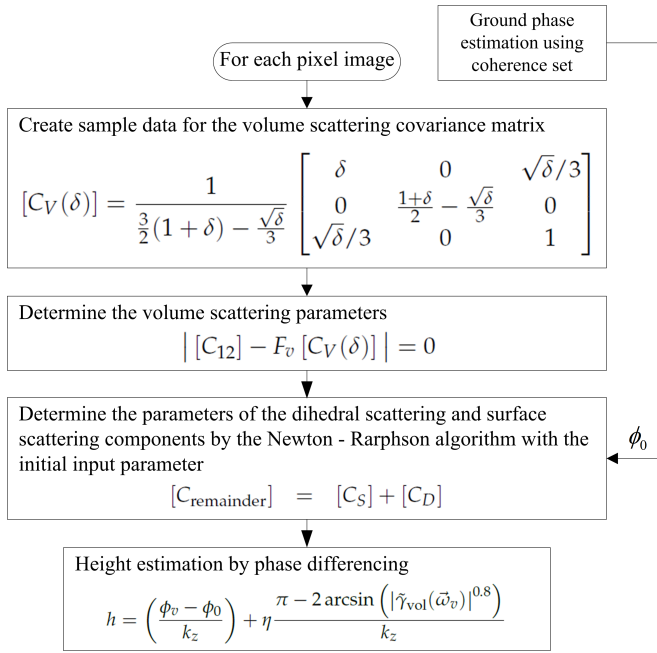


Figure 1. Improved adaptive decomposition algorithm for single pixel.

As can be seen in matrix $[C_{\text{remainder}}]$, there appear four complex unknowns and four complex observables, since $C_{\text{remainder}(1,3)} \neq C_{\text{remainder}(3,1)}$. Equation (19) lead to a determined nonlinear equation system. Therefore, to determine the rest of unknown parameters α , β , F_D , F_S simultaneously, a Newton-Raphson algorithm is implemented. Hence, power contribution for surface and double bounce component can be estimated as in [4]. Assuming that the double-bounce mechanism is located at ground level [5], the topographical phase is therefore regarded as the phase of F_D . So, the double-bounce scattering phase is used as the initial input parameter to the Newton-Raphson algorithm, which, in turn, is used to solve the nonlinear equation system for target decomposition.

Finally, we repeat both above steps for each pixel in image. After retrieving F_S , F_D and, F_V , the forest height by phase differencing can be expressed as:

$$h_v = \frac{\phi_v - \phi_0}{k_z}, \quad (20)$$

where k_z , ϕ_v , ϕ_0 are vertical wave number, canopy phase and surface phase respectively.

However, phase centre can lie any where between halfway and top of the layer, and hence in general the true height is underestimated. This can be overcome by employing a coherence amplitude correction term. By combining these two terms with a scaling parameter η , we then obtain an accurate height algorithm that can compensate variation in structure, as shown in Equation (21):

$$h = \left(\frac{\phi_v - \phi_0}{k_z} \right) + \eta \frac{\pi - 2 \arcsin \left(|\tilde{\gamma}_{\text{vol}}(\tilde{\alpha}_v)|^{0.8} \right)}{k_z} \quad (21)$$

The first term represents the phase coherence while the second term is the coherence amplitude correction.

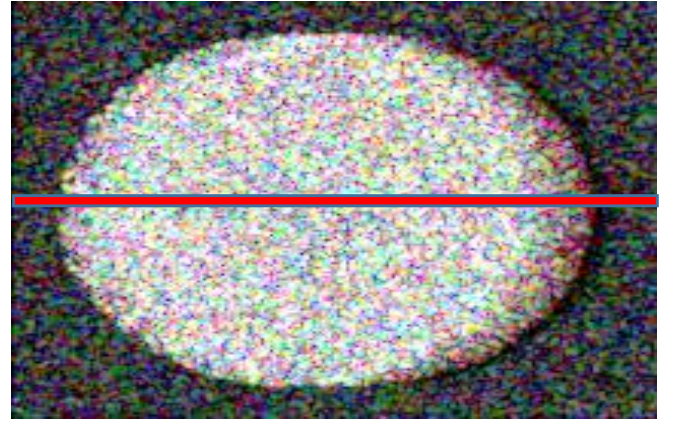


Figure 2. Pauli image on RGB coding of the RVoG stand.

This expression has the right kind of behavior in two important special cases. If the medium has a uniform structure function, the first term will give half the height but the second will then also obtain half the true height (if we set $\eta = 0.5$). At the other extreme, if the structure function in the volume channel is localized near top of the layer, then phase height will give the true height, and the second term will approach zero. That is the reason why the weight is set as $\eta = 0$. To reduce the error from change of extinction coefficient and the vertical structure, we select $\eta = 0.4$ [13].

The algorithm of scattering component estimation is summarized in Figure 1.

4 EXPERIMENTAL RESULT

To illustrate the technique, we shall apply the improved three-component decomposition algorithm to a data set acquired from PolSARProSim software by Mark L. Williams [14], as well as a pair of L-band PolInSAR images of Tien-shan test site by the SIR-C/X-SAR system.

4.1 Simulated Data

First, we attempted to validate the proposed algorithm by using simulated PolSARProSim data. The PolSARProSim calculates simulated SAR imagery of model forest stands. We simulated an L-band scenario, which is named HEDE, with a forest height of 10 m, at 1.3 GHz and at 30 degree angle of incidence considering different soil conditions and averaging window sizes. The azimuthal slope is 0.1%, whereas the range slope is 0.2%. The interferometer is operated at 10.6 m horizontal and -6.1 m vertical baseline. The forest stand occupies a 0.7854 Ha area and stand density is 360 stem/Ha. Azimuth and slant range resolution are 1.0 m and 0.5 m, respectively.

Figure 2 shows a red, green, blue (RGB) coding Pauli image of the RVoG scenario considered with 181 pixels in range and 215 pixels in azimuth, and the red line indicates the transection analyzed in this section.

Figure 3 is a plot of the forest height estimation of the proposed approach compared with the three-stage inversion process along the transect line.

Table I
FOREST HEIGHT ESTIMATION FOR TWO APPROACHES.

Parameter	Forest height h_v [m]	Ground phase ϕ_0 [rad]	Average errors [m]	RMSE (h_v) [m]
True	10	-0.148	0	0
Three - stage inversion	8.5676	-0.1160	1.4324	2.7052
Proposed method	9.6800	-0.1350	0.3200	2.5641

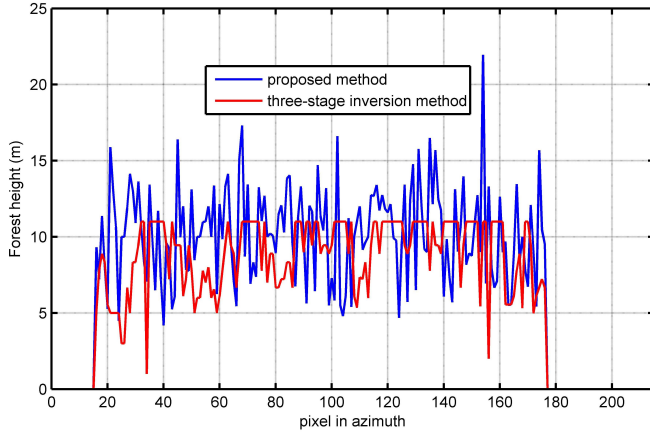


Figure 3. Plot of the height extraction comparison.

Table I indicates forest height estimation by using the proposed method and three stage inversion process. Compared with the actual 10 m tree height, Figure 3 and Table I indicate that the proposed approach is more accurate and has fewer errors than the three-stage inversion method. In the three-stage inversion method, the inversion of forest height can be divided into three stages. The ground phases are extracted in the first two stages by using the line fit method. The forest heights are estimated in the last stage. In these stages, we usually assume that there is not any ground scattering component in the HV channel, and let volume decorrelation be $\tilde{\gamma}_{est,v} \approx \tilde{\gamma}_{HV} \exp(-j\phi_0)$. We can construct a look-up table (LUT) of volume coherence $\tilde{\gamma}_{vol}$ as a function of forest height h_v and the extinction coefficient σ . By comparing $\tilde{\gamma}_{est,v}$ with the LUT, we can then obtain the forest height estimation. When $\tilde{\gamma}_{est,v} \approx \tilde{\gamma}_{vol}$, forest height will be assigned to the given value. Thus, in Figure 3, approximate height values are assigned to a given value and this is the cause of the upper threshold value. Additionally, this method requires that the vertical structure and the temporal decorrelation are neglected and the minimum ground-to-volume scattering ratio needs to be lower than -10 dB to secure around 10% accuracy [15]. The accuracy of estimating these parameters depends on model predictions [5, 16]. Therefore, the estimation of forest height and extinction by using three-stage method are not reliable. Based on mathematical basis, the proposed method detected the volume scattering after applying the Freeman-Durden decomposition technique. So, the accuracy of canopy phase estimation is improved remarkably. We can say that the forest height estimation by using improved three-component

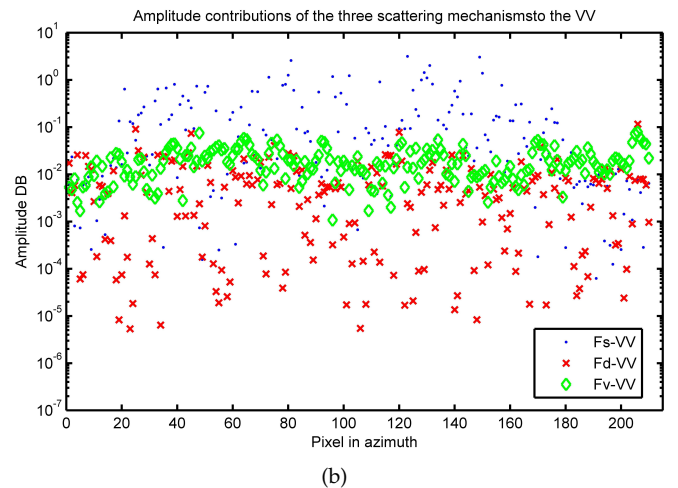
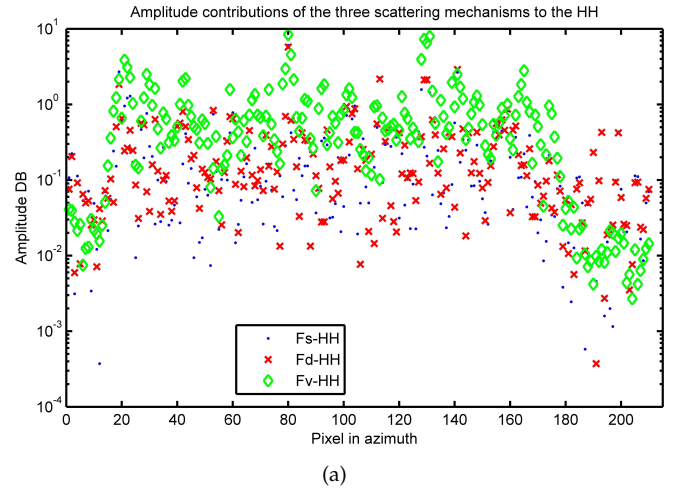


Figure 4. Amplitude contributions of three scattering mechanisms to (a) HH and (b) VV with highest roughness

decomposition technique is more accurate and reliable than its by using three-stage inversion process.

Figure 4 corresponds to the amplitude of the three scattering mechanisms contributing to the HH (4a) and VV (4b) channel. As shown, in both HH and VV channel, the amplitude response is dominated by the volume scattering but the double-bounce scattering component is also remarkable. In addition, the double-bounce scattering component is low for the VV correlation (as predicted by theory), and it is not dominant in the HH channel.

The forest height estimation of the volume scattering and surface scattering component along transection line are shown in Figure 5. We show that almost all height estimation of surface scattering are very low. However, they have height greater than zero at some pixels due

Table II
PARAMETERS ESTIMATION FOR TWO DIFFERENT SCENES USING PROPOSED METHOD.

	Scene 1 (DECIDUOUS)		Scene 2 (PINE)	
	True	Proposed method	True	Proposed method
Ground Phase ϕ_0 [rad]	0.0212	0.0306	-0.0136	-0.0224
Forest height h_v [m]	10	10.2364	15	15.4465
Average errors [m]	0	0.2364	0	0.4465
RMSE (h_v) [m]	0	1.7716	0	2.5875

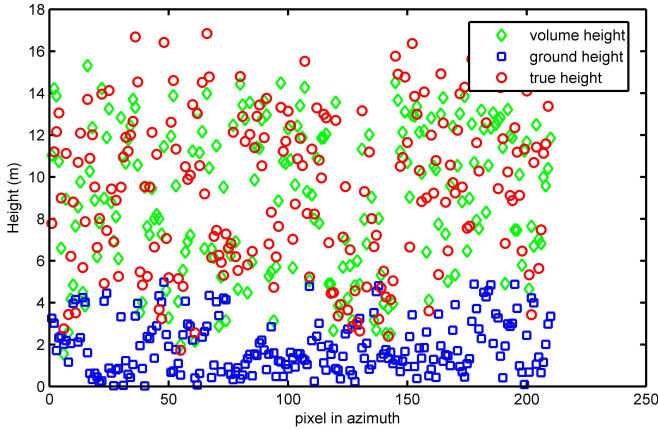


Figure 5. The forest height estimates for two scattering components.

to the soil roughness, moisture conditions and terrain slope. This figure shows that the actual forest heights are quite well retrieved. The forest height estimation of the volume scattering are in the range of 5 to 15 m and have an average value of approximately 10 m. Therefore, the forest heights are very accurately estimated.

The result of the proposed method is shown in Figure 6. In this figure, it is shown that almost the peaks of the height are located at approximately 10 m. The actual forest heights are quite well retrieved, except some pixels are overestimated but all of the forest heights in these pixels are less than 22 m. Hence, we can say that the results are acceptable. Consequently, the proposed method provides relative accuracy with small error, and is more accurate for vertical structural variations.

Changes in the scene parameters can be noticed by means of the proposed approach. Table II shows the estimation of forest parameters when tree species is PINE and DECIDUOUS. When different tree species are used, the attenuation of electromagnetic through the canopy layer becomes stronger, and the direct ground backscatter that grows into it is also noticeable. Therefore, the forest height and ground phase become overestimated, but these results approximate true values. From Table II, we can say that the forest height and ground phase estimation by using the proposed method is accurate and reliable.

4.2 Space Borne PolInSAR Data

In this section, the proposed algorithm is also tested with space-borne data. The data set using for testing

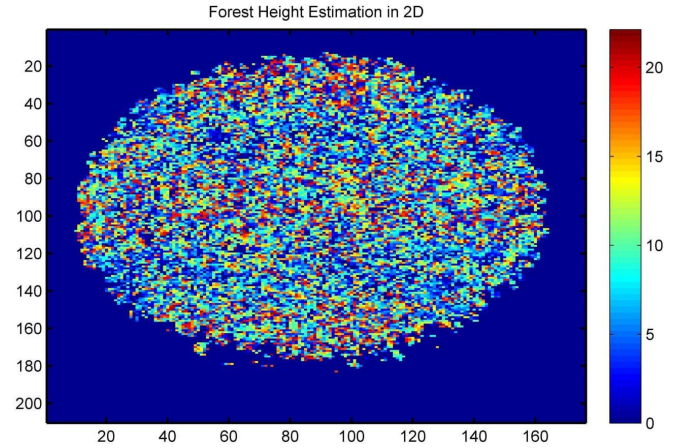


Figure 6. The forest height is estimated by proposed algorithm.

proposed method is acquired from a pair of SIR-C single look complex (SLC) images of the Tien-shan test site by the SIR-C system. This region has a mixed forestry, road and agricultural area. They consist of quad-pol interferometric data at L-band with a 24.569 degree angle of incidence and 13 m baseline.

Figure 7(a) is the optical image of the test site, Figure 7(b) is a composite image of the test site in the Pauli basis, with 500 pixels in range and 500 pixels in azimuth. The analysis has been performed on the azimuth transect. Along this transect, we can identify three types of scenes: red areas denote bare surfaces like agriculture and road, green areas represent forest.

The amplitude contributions of the three scattering mechanisms are shown in Figure 8(a) and 8(b). For the VV-pol cross-correlation channel, the volume scattering is the most dominant source of scattering. For the HH-pol cross-correlation channel, the double-bounce mechanism is relatively high but it is not dominant due to the relative roughness of terrain, volume scattering is also dominant in forested areas. In comparison with the VV channel, double-bounce scattering increased. This is consistent with the definition of Fresnel coefficients, in which the HH contribution exceeds the VV contribution.

Figure 9(a), 9(b) and 9(c) show the decomposed power images of surface (P_s), double-bounce (P_d) and volume scattering (P_v) of the data by the proposed algorithm respectively. In figure 9(b), we found out that, the double-bounce scattering components in boundary forest and road areas are stronger than those of the forest and agricultural areas. In contrast, the volume

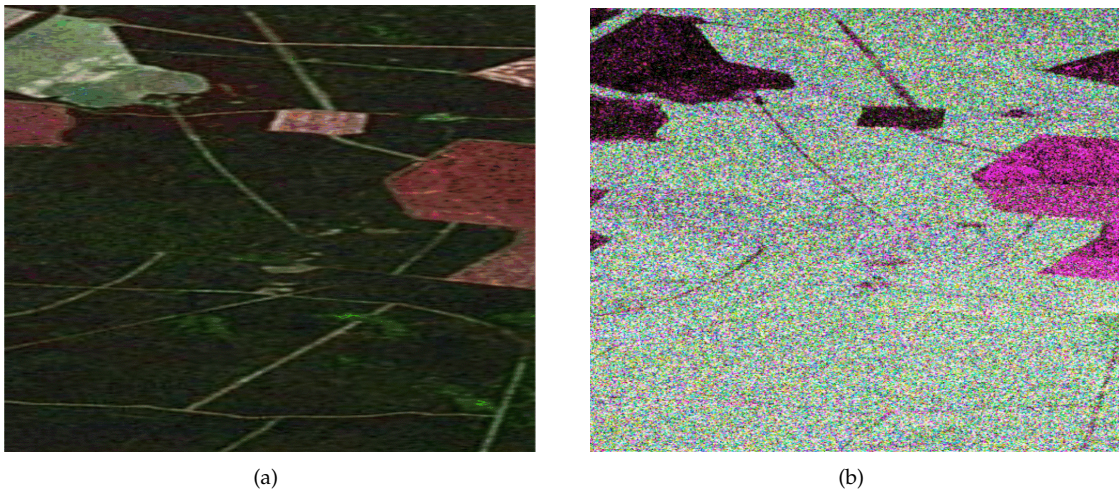


Figure 7. The Test site in Tien-Shan: a) Optical image b) Pauli decomposition of test site.

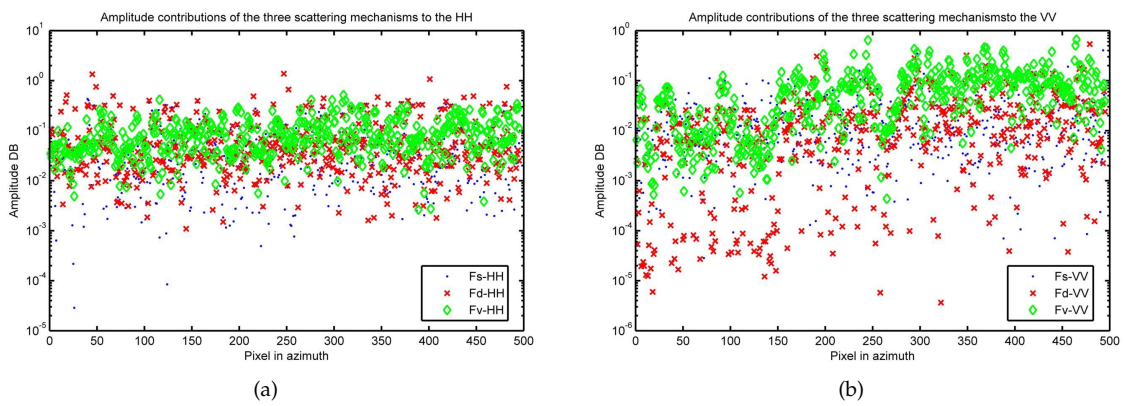


Figure 8. Amplitude contributions of the three scattering mechanisms to the (a) HH, (b) VV cross correlation.

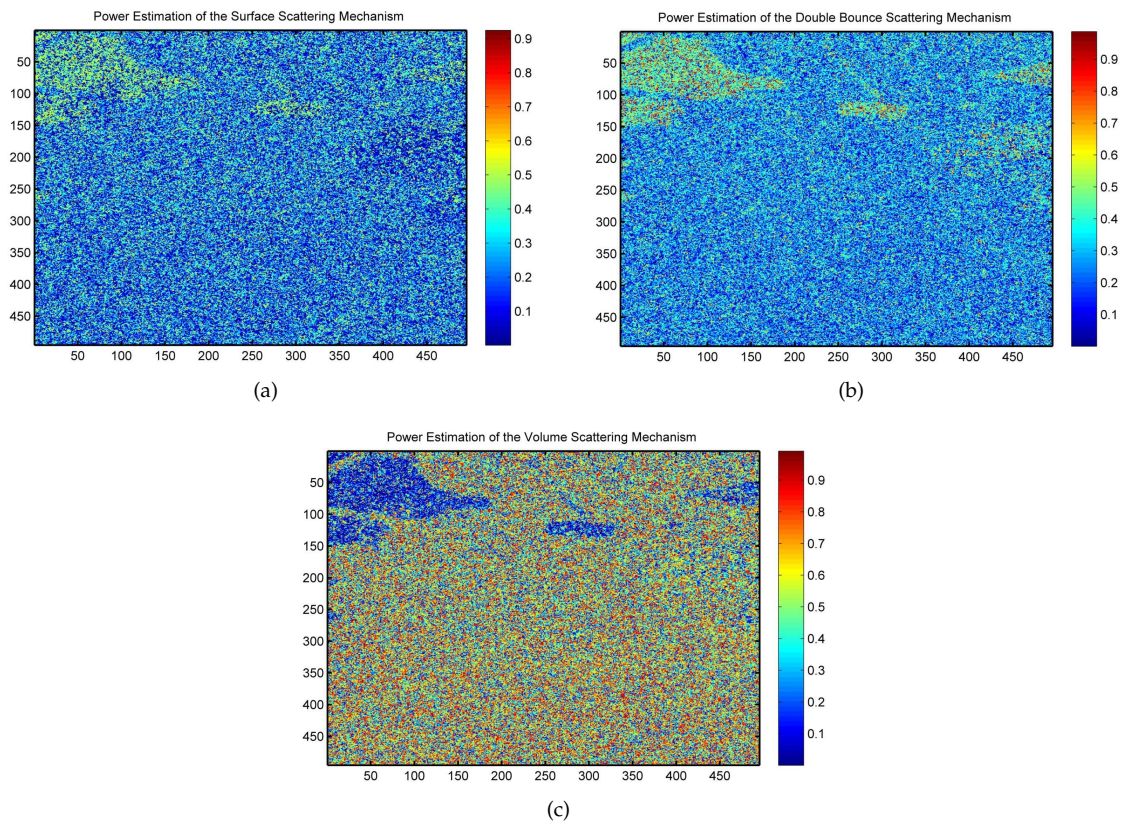


Figure 9. Results of the improved three-component decomposition. (a) Power image of PS , (b) Power image of PD and (c) Power image of PV.

Table III
FOREST PARAMETERS ESTIMATION FOR EVALUATION AREA.

Average height [m]	Fraction fill canopy (r_h)	RMSE (h_v) [m]	Ground phase [rad]
18.1940	0.4250	4.4986	0.0081

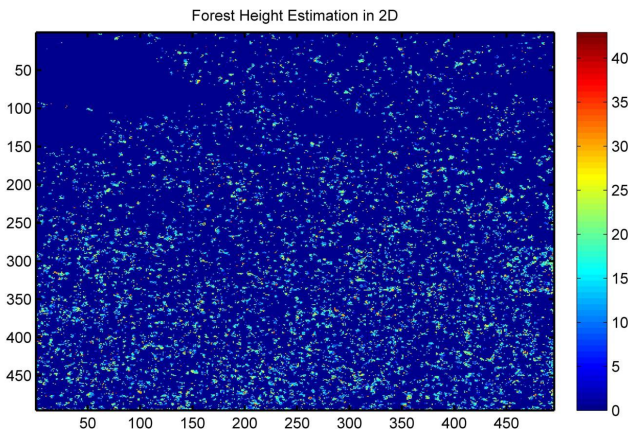


Figure 10. The forest height is estimated by proposed algorithm.

scattering components are more intense in forest and agricultural areas, as we observe in Figure 9(c).

The result of the proposed algorithm is shown in Figure 10. Comparing Figure 10 with Figure 7(a), we found out that, the height is estimated to be very low in the road areas. This result is consistent with the actual terrain.

Figure 11 shows a three-dimensional perspective of the estimated height by the proposed algorithm. In this figure, it is shown that almost the forest height is located in the range between 12 m and 30 m. The mean forest height is 18.1940 m. Table III shows the forest height estimation using the proposed method for the test site area.

5 CONCLUSION

In this paper, an accuracy enhancement method of vegetation height estimation using the improved three-component decomposition technique has been proposed. The accurate topographical phase of forest areas has been estimated by coherence set. This phase was then used as the initial input parameter of the Newton-Raphson method. By using this method, we can not only obtain relative accuracy for height estimation but also estimate power contributions of each scattering component. Simulated and spaceborne data have been used for testing the proposed algorithm and its potential has been analyzed also in comparison with the three-stage inversion method for height estimation. These preliminary results show that the proposed model is effective for analysis of forest areas with PolInSAR image. Experimental results indicate that vegetation parameters can be retrieved directly and accurately. In the future, more experiments using different data of different fields will be done and the enhancement performance of proposed algorithm will be studied.

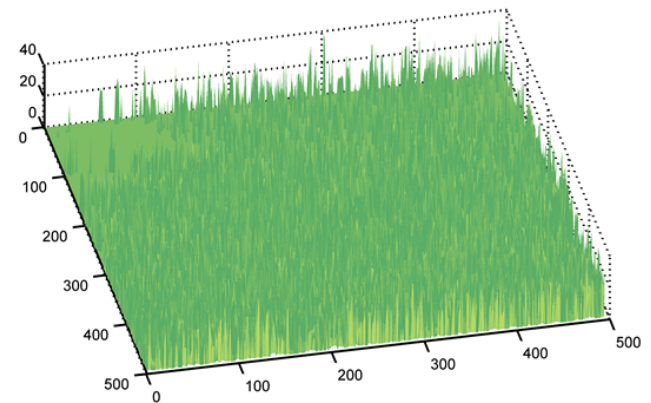


Figure 11. 3-D view of forest height.

ACKNOWLEDGMENT

This research is funded by Vietnam National Foundation for Science and Technology Development (NAFOSTED) under grant number 102.01-2017.04

REFERENCES

- [1] S. R. Cloude and K. P. Papathanassiou, "Polarimetric optimisation in radar interferometry," *Electronics Letters*, vol. 33, no. 13, pp. 1176–1178, 1997.
- [2] —, "Polarimetric SAR interferometry," *IEEE Transactions on Geoscience and Remote Sensing*, vol. 36, no. 5, pp. 1551–1565, 1998.
- [3] H. Yamada, Y. Yamaguchi, Y. Kim, E. Rodriguez, and W.-M. Boerner, "Polarimetric SAR interferometry for forest analysis based on the ESPRIT algorithm," *IEICE Transactions on Electronics*, vol. 84, no. 12, pp. 1917–1924, 2001.
- [4] H. Yamada, M. Yamazaki, and Y. Yamaguchi, "On scattering model decomposition of polsar image and its application to the esprit-based pol-insar," in *Proceeding of the 6th European Conference on Synthetic Aperture Radar*, 2006.
- [5] S. R. Cloude and K. P. Papathanassiou, "Three-stage inversion process for polarimetric SAR interferometry," *IEEE Proceedings-Radar, Sonar and Navigation*, vol. 150, no. 3, pp. 125–134, 2003.
- [6] B. Zou, D. Lu, H. Cai, and Y. Zhang, "Ground topography estimation over forests using polinsar image by means of coherence set," in *18th IEEE International Conference on Image Processing (ICIP)*. IEEE, 2011, pp. 2809–2812.
- [7] J. D. Ballester-Berman and J. M. Lopez-Sanchez, "Applying the freeman–durden decomposition concept to polarimetric sar interferometry," *IEEE Transactions on Geoscience and Remote Sensing*, vol. 48, no. 1, pp. 466–479, 2010.
- [8] —, "Application of freeman–durden decomposition to polarimetric sar interferometry," in *8th European Conference on Synthetic Aperture Radar (EUSAR)*. VDE, 2010, pp. 1–4.
- [9] M. Arii, J. J. van Zyl, and Y. Kim, "Adaptive model-based decomposition of polarimetric sar covariance ma-

- trices," *IEEE Transactions on Geoscience and Remote Sensing*, vol. 49, no. 3, pp. 1104–1113, 2011.
- [10] J. J. Van Zyl, M. Arii, and Y. Kim, "Model-based decomposition of polarimetric sar covariance matrices constrained for nonnegative eigenvalues," *IEEE Transactions on Geoscience and Remote Sensing*, vol. 49, no. 9, pp. 3452–3459, 2011.
- [11] O. Antropov, Y. Rauste, and T. Hame, "Volume scattering modeling in polsar decompositions: Study of alos palsar data over boreal forest," *IEEE Transactions on Geoscience and Remote Sensing*, vol. 49, no. 10, pp. 3838–3848, 2011.
- [12] M. Neumann, A. Reigber, and L. Ferro-Famil, "Polinsar coherence set theory and application," in *European Conference on Synthetic Aperture Radar EUSAR. Dresden, Germany*, 2006.
- [13] S. R. Cloude, "Pol-insar training course," *Radio Science*, 2005.
- [14] M. Williams, "Polsarprosim: a coherent, polarimetric sar simulation of forest for polsarpro," <http://earth.eo.esa.int/polsarpro/SimulatedDataSources.html>, 2006.
- [15] J. Chen, H. Zhang, and C. Wang, "Comparison between esprit algorithm and three-stage algorithm for polinsar," in *International Conference on Multimedia Technology (ICMT)*. IEEE, 2010, pp. 1–3.
- [16] N. P. Minh, B. Zou, Y. Zhang, and V. Le, "General three-layer scattering model for forest parameter estimation using single-baseline polarimetric interferometry synthetic aperture radar data," *Journal of Applied Remote Sensing*, vol. 9, no. 1, pp. 1–18, 2015.



Nguyen Ngoc Tan was born in 1986. He received B.S. degree from the Posts & Telecommunication Institute of Technology, Hanoi, Vietnam in 2012 and M.S. degree from the Le Quy Don Technical University, Hanoi, Vietnam in 2014. Now he is working for CMC Telecom Company, Pham Hung Street, Cau Giay district, Hanoi. He currently focuses on digital signal processing, signal sonarprocessing, polarimetric SAR, polarimetric SAR interferometry.



Pham Minh Nghia was born in 1980. He received the B.S., M.S. degrees in electronics engineering from the Le Qui Don Technical University, Vietnam, in 2005 and 2008, respectively, and the Ph.D. degree in information and communication engineering from the Harbin Institute of Technology, China in 2014. He is currently a lecturer at Le Qui Don Technical University and visiting lecturer at Duy Tan university, Vietnam. He currently focuses on polarimetric synthetic aperture radar

image processing, polarimetric SAR interferometry and signal processing.



Bui Ngoc Thuy was born in 1978. He received the B.S, M.S degrees in electronics engineering from the Le Qui Don Technical University, Vietnam, in 2002 and 2010. He is currently a lecturer at Tran Dai Nghia University. He currently focuses on polarimetric synthetic aperture radar image processing, polarimetric SAR interferometry and Ph.D. student at Military science and technology institute.